Electronic structures, surface phonons, and electron-phonon interactions of Al(100) and Al(111) thin films from density functional perturbation theory

Gui Qin Huang
Department of Physics, Institute of Theoretical Physics, Nanjing Normal University, Nanjing, Jiangsu 210097, People's Republic of China

(Received 1 August 2008; published 29 December 2008)

The evolution of electronic structures, surface phonons, and electron-phonon interactions with the slab thickness in Al(100) and Al(111) films is studied from density functional perturbation theory. Our results clearly show a periodic oscillatory behavior of the calculated interlayer relaxations, surface energies, total density of states at the Fermi level, surface phonon states, electron-phonon coupling constant λ, and even the transition temperature T_C of superconductivity as a function of the slab thickness for Al(111) films. However there is no clear periodic oscillation found for Al(100) films. The different oscillatory behavior of physical properties between Al(111) and Al(100) films is discussed by considering the crystal band structure. For both Al(111) and Al(100) slabs, the values of λ and T_C obtained in this work at small slab thickness greatly exceed their bulk values. Both electronic confinement and the softening of surface phonons contribute to the enhancement of superconductivity for films at small thickness.

DOI: 10.1103/PhysRevB.78.214514 PACS number(s): 74.78.Db, 63.20.kd, 63.20.dk, 63.22.Np

I. INTRODUCTION

In an ultrathin metallic film, electrons move quasifreely in the lateral planes, while their motion in perpendicular direction to the film surface is confined, causing electronic states quantized into the well-known quantum well (QW) states. A variety of physical properties would exhibit quantum oscillatory behavior as a function of the film thickness due to quantum size effect, including conductivity,[1] electronic structure,[2,3] Hall coefficient,[4] thermal expansion,[5] work function,[6] surface reactivity,[7] thermal stability,[8] etc. Especially, some experimental evidences have shown the existence of quantum size effect in the ultrathin superconducting films. In early investigation,[9] it was estimated that the regions of film which exhibit the greatest increase in T_C are within a few monolayers in both Al and Sn. Very recently, using atomically uniform film of lead with exactly known numbers of atomic layers deposited on a silicon (111) surface, Guo *et al.*[10] observed oscillations in T_C. Using a scanning tunneling spectroscopy, Eom *et al.*[11] observed that both energy gap and transition temperature exhibit persistent oscillation without any suppression at ultrathin Pb films. This means that one is allowed to control the film thickness at the atomic scale for the desired superconducting properties.

For a conventional superconductor, electron-phonon (EP) interaction is ultimate to bind the Cooper pairs. Experimentally, EP effects are becoming increasingly accessible on surfaces and films through powerful techniques such as high-resolution angular-resolved photoemission spectroscopy, scanning tunneling spectroscopy, and time-resolved two-photon photoemission spectroscopy. Guo *et al.*[10] observed that the oscillatory behavior of T_C correlated well with the electron density of states (DOS) near the Fermi level and the EP coupling. Several groups observed the oscillatory variation in the EP coupling constant as a function of film thickness and reported an enhancement of the EP coupling parameter at small film thicknesses.[12,13] The first parameter-free *ab initio* calculation of the EP interaction has been reported at a real metal surface, Be(0001).[14] Recently, Yndurain and Jigato[15] do a first-principles calculation for Pb(111) slabs; they found that the frequency of localized surface phonons and the deformation potential for the lowest unoccupied and the highest occupied quantum well states have an oscillatory behavior with a bilayer periodicity. However, their calculations are limited to the phonons at $K_{//}=0$.

The present paper studies electronic structures, surface phonons, and electron-phonon interactions of Al(100) and Al(111) films by first-principles calculations. We focus on the study of the dependence of surface localized phonons, EP interactions, and even superconducting transition temperatures as a function of the film thickness by considering all phonons and all electronic states. This has not been studied so far by first-principles calculation to the best of the author's knowledge.

II. COMPUTATIONAL METHOD

The calculations have been performed within the density functional perturbation theory[16] in a plane-wave pseudopotential representation through the PWSCF program.[17] The ultrasoft pseudopotential[18] and general gradient approximation–Perdew-Burke-Ernzerhof (GGA-PBE) (Ref. 19) for the exchange and correlation energy functional are used with a cutoff of 25 Ry for the expansion of the electronic wave function in plane waves. The Al films are modeled using the slabs which are separated by about seven atomic layers of vacuum. In all the calculations below, a surface (1×1) unit cell is employed for the supercell slab. For the electronic structure calculations, the Brillouin-zone integrations are performed with a (16,16,1) grid by using the first-order Hermite-Gaussian smearing technique.[20] Within the framework of the linear-response theory, the dynamical matrices and the electron-phonon interaction coefficients are calculated for (8,8,1) grid of special **q** points in the two-dimensional irreducible Brillouin zone. The dense (32,32,1)

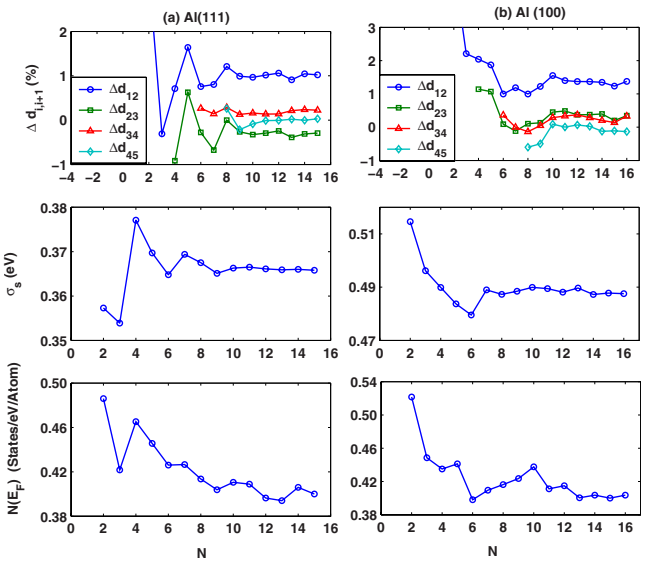

FIG. 1. (Color online) Interlayer relaxations $\Delta d_{i,i+1}$, surface energies σ_s, and total DOS at the Fermi level per Al atom $N(E_F)$ as a function of the number of layers N in the slab (a) for Al(111) and (b) for Al(100).

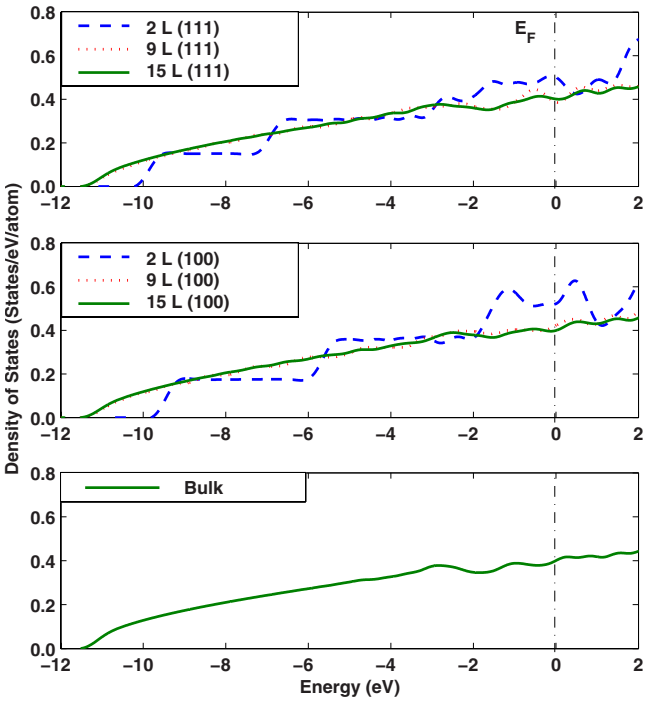

FIG. 2. (Color online) The total density of states for the Al(111) and Al(100) films with a different number of layers as well as for the bulk. For convenience, the Fermi level $E_F=0$ is taken.

grid is used in the Brillouin-zone integrations in order to produce the accurate EP interaction matrix.

The energy and frequency convergence are carefully checked. After setting the smearing parameter to 0.05 Ry, the electronic total energies are converged within 0.02%, while the phonon frequencies are converged within 3 cm^{-1} with respect to the cutoff energy and k-point sampling. The size of the vacuum region is also checked. When adding one more atomic layer for the region of vacuum, the changes in frequencies are less than 1 cm^{-1}. So, seven atomic layers of vacuum are sufficient to decouple the two surfaces across the vacuum.

III. RESULTS AND DISCUSSION

The bulk Al lattice constant is first optimized via the total-energy minimization. The obtained lattice constant $a=7.61$ a.u., which is in good agreement with other theoretical result.[2] This theoretical bulk value is used for the in-plane lattice constant of the freestanding Al(100) and Al(111) films. Starting from an ideal surface, the relaxation is performed by minimizing the total energy with respect to the atomic positions in the slab. When the force on each atom is smaller than 10^{-4} Ry/a.u., we assume that the atoms are in their equilibrium positions. The calculated interlayer relaxations $\Delta d_{i,i+1}$ are plotted in Fig. 1. Here $\Delta d_{i,i+1}$ is given by $\Delta d_{i,i+1}=100(d_{i,i+1}-d_0)/d_0$. $d_{i,i+1}$ is the interlayer distance between two adjacent layers and d_0 is the unrelaxed interlayer distance. $d_0=\sqrt{3}a_0/3$ and $a_0/2$ for (111) and (100) slabs, respectively. The present results agree well with recent calculations based on the full-potential linearized augmented plane-wave (FLAPW) method.[2] For Al(111) slabs, the magnitude of the relaxations oscillates as a function of the number of layers. From Fig. 1(a), we can see that the oscillation period is about three layers. However there is no clear periodic oscillation found in Fig. 1(b) for Al(100) slabs.

Figure 2 shows the total DOS per Al atom for the fully relaxed Al(111) and Al(100) films as well as for the bulk. For convenience, the Fermi level $E_F=0$ is taken. The DOS curves are in good agreement with the results in Ref. 2. When $N=2$, steplike function is clearly seen at the onset of DOS curve because of two-dimensional periodicity. For both two films, the DOSs for $N=9$ and $N=15$ layers are almost identical and quite similar to that in the bulk except that some tiny differences appear in the vicinity of Fermi level.

The total DOS at the Fermi level per Al atom $N(E_F)$ and surface energies σ_s are calculated and also plotted in Fig. 1 for the fully relaxed Al(111) and Al(100) films. The surface energy in Fig. 1 is defined as one-half of the energy difference between the film and the bulk with the same number of atoms. The reference bulk total energy is obtained by a linear fitting of the slab total energies, which was suggested in Ref. 21. The convergent surface energies are 0.37 and 0.49 eV for Al(111) and Al(100) films, respectively, which are in good agreement with those reported by FLAPW method (0.36 and 0.48 eV, respectively).[2] Both the surface energy and the total density of states at the Fermi level oscillate with the period of about three layers for Al(111) films. However, the same behavior is not clearly found for Al(100) films. These differences between Al(111) and Al(100) films will be discussed by considering the crystal band structure in the following. The first-principles calculations by Wei and Chou[22] show that a quantitative description of the quantum size effect in Pb(100) thin films requires full consideration of the crystal band structure.

The Al bulk band dispersions along several directions are shown in the right panel of Fig. 3. The surface Brillouin

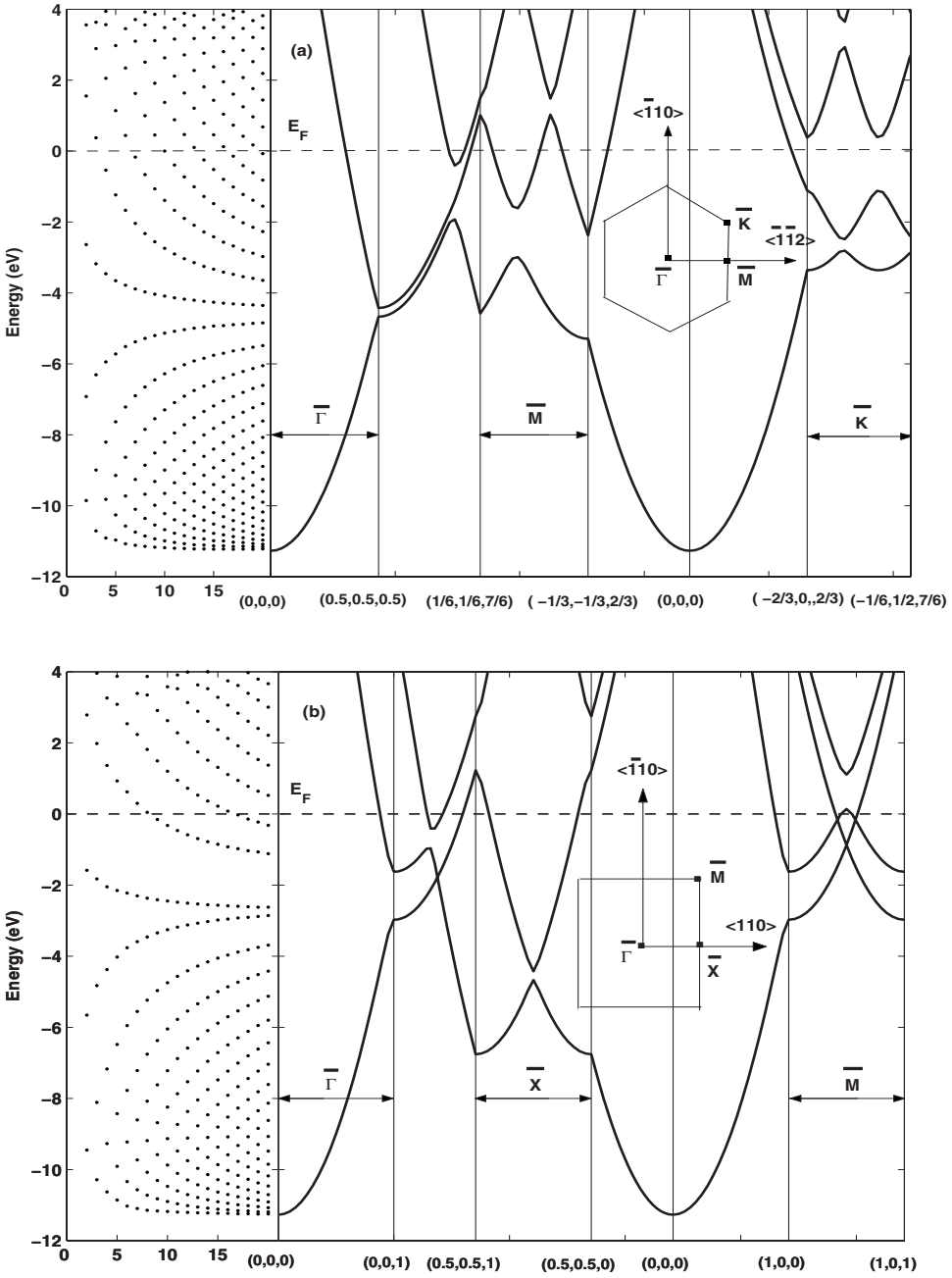

FIG. 3. The bulk band structure of Al along several directions. The surface Brillouin zones of a fcc (111) and a fcc (100) lattice with the high-symmetry points are shown in the inset of (a) and (b), respectively. The calculated QW levels at $\bar{\Gamma}$ point as a function of Al(111) and Al(100) slab thicknesses are plotted in the left panel of (a) and (b), respectively. The energy zero is set at the Fermi energy of each film.

zones of fcc (111) and (100) lattices are shown in the inset of Fig. 3. The high-symmetry points of the surface Brillouin zone onto which the bands will be projected are also labeled in Fig. 3.

For Al(111) films, we will focus on the band dispersions along the [111] direction in Fig. 3(a). The bands from (0,0,0) to (0.5,0.5,0.5) will be projected onto $\bar{\Gamma}$ point of (111) surface Brillouin zone and determine the energy range of QW states there. There is one band cutting through the Fermi level along this direction. The bottom of this band is at (0.5,0.5,0.5) point. According to the quantization condition,[23] the periodicity of the QW states crossing the Fermi level is roughly equal to π/k_F, where k_F is the bulk Fermi wave vector in the film normal direction. The measured k_F from (0.5,0.5,0.5) point is $k_F=0.31\pi/d_0 \approx \pi/(3.2d_0)$, suggesting a periodicity of three monolayers. However this Fermi wave vector $k_F=0.44\pi/d_0 \approx \pi/(2.2d_0)$ in Pb,[24] explaining a bilayer oscillating period of some physical properties in Pb(111) films. From $(-2/3,0,2/3)$ to $(-1/6,1/2,7/6)$, there is no band crossing the Fermi level. So the QW states produced at $\bar{K}$ do not contribute to the oscillating behavior of various properties of Al(111) films. The band crossing the Fermi level along $(-1/3,-1/3,2/3)$ to (1/6,1/6,7/6) direction and projected onto $\bar{M}$ of (111) surface Brillouin zone comes from the same origin as the projected band at $\bar{\Gamma}$ near the Fermi level. This is a hole-type band. From the position where the band crossing the Fermi level to the top of this band, the hole Fermi wave vector $k_F'=0.115\pi/d_0 \approx \pi/(8.7d_0)$, suggesting that a new QW hole state will appear when the film thickness increases by approximately nine monolayers. This will have small effect on the oscillation of the physical properties. So, the quantum size effect of

Al(111) films is mainly determined by the QW states at $\bar{\Gamma}$ point. The oscillatory behavior of Al(111) films is weaker than that of Pb films due to their different crystal band structures. The band structures of Pb in the vicinity of Fermi level are simpler than those of Al. The bands which will be projected onto $\bar{K}$ and $\bar{M}$ points do not cross the Fermi level, so the quantum size effect of Pb(111) films is completely determined by the QW states at $\bar{\Gamma}$ point.

For Al(100) films, we look at the band dispersions along the [100] direction in Fig. 3(b). The bands from (0,0,0) to (0,0,1) will be projected onto $\bar{\Gamma}$ point of (100) surface Brillouin zone. There is one band cutting through the Fermi level along this direction. The measured k_F from (0,0,1) point is $k_F=0.113\pi/d_0 \approx \pi/(8.8d_0)$, suggesting a periodicity of nine monolayers. However, it can be seen that the band structures near the Fermi level along the [100] direction are more complicated than those along the [111] direction. The band crossing the Fermi level from (0,0,0) to (0,0,1) direction and that from (0.5,0.5,0) to (0.5,0.5,1.0) direction are two different bands. So the QW states near the Fermi level at $\bar{\Gamma}$ and at $\bar{X}$ have different origins. Furthermore, we notice that there are two different bands crossing the Fermi level from (1,0,0) to (1,0,1) direction. So there are two kinds of QW states near the Fermi level at $\bar{M}$ point. We think that the complicated situation of QW filling near the Fermi level results in no clear oscillatory period in the physical properties of the Al(100) film.

The QW levels at $\bar{\Gamma}$ point as a function of Al(111) and Al(100) slab thicknesses are plotted in the left panel of Fig. 3. The energy zero is set at the Fermi energy of each film. For Al(111) and Al(100) films, respectively, we can see that a new QW level appears below the Fermi level for every incremental increase in about three monolayers and nine monolayers in the film thickness, consistent with the above Fermi wavelength analysis.

The phonon dispersion in a thin film is very different from that in the bulk, and a quantization of the phonon spectrum occurs. The change in geometry and the redistribution of the electronic charge will change the effective potential and in general cause the appearance of surface modes. In order to identify which ones of the calculated slab modes have a dominant surface character, we have calculated their localization rate, defined as

$$l(\nu,\vec{\mathbf{q}}) = \frac{\sum_{\alpha,n} u_{\alpha,n}(\nu,\vec{\mathbf{q}})^2}{\|\mathbf{u}(\nu,\vec{\mathbf{q}})\|^2}, \quad (1)$$

where α is the polarization index, $\mathbf{u}(\nu,\vec{\mathbf{q}})$ is the amplitude of the atomic displacements for the νth normal mode at the wave vector $\vec{\mathbf{q}}$, and the sum runs over α and the number of atoms of the two topmost layers of each side of the slab.

Results of the localized surface phonon modes for the fully relaxed 12-layer (111) slab and 13-layer (100) slab are shown in Fig. 4. The light gray lines represent the projected bulk phonon dispersions. The modes for which the localization rate is larger than 40% are indicated with open circles and filled squares localizing in the first and second layers, respectively. In Ref. 25, the surface phonon-dispersion curves of Al(100) are obtained by first-principles calculation and the polarization characters of the surface phonon modes are analyzed in detail. Our calculated surface modes agree very well with the results in Ref. 25. In Fig. 4(a), we have adopted the same notation for surface modes in (100) slab as in Ref. 25. S_1, S_7, and S_2 are surface modes localized in the topmost layer, while S_2' is a subsurface mode. S_1 is Rayleigh mode and polarized normal to the surface. S_7 and S_2 are shear-horizontal and shear-vertical components, respectively. In Fig. 4(b), the surface modes in (111) slab are labeled using the nomenclature of Ref. 26. As in (100) slab, the lowest surface-mode branch S_1 which lies below the bulk bands is the Rayleigh wave. The gap mode S_3 is primarily a shear-horizontal mode. The surface mode S_2 is primarily a longitudinal mode. S_5 is a subsurface mode. Furthermore, the gap mode S_4 which its localization rate is smaller than 40% is also shown in Fig. 4(b) with cross points. The calculated frequencies of surface modes at some high-symmetry points are summarized in Table I, together with the results in other references. Our results are found to be close both to the experimental data and to the results of other calculations.[25,27–30]

In lattice-dynamical slab calculations, surface modes appear at both slab surfaces. These modes have different frequencies because of the interaction between the two surfaces. The wider the slab becomes, the smaller the difference of frequency is and they will have the same frequency in a hypothetical infinite slab. The frequencies of localized surface phonon modes as a function of the number of layers N in the slab are sketched in Fig. 5. From Fig. 5(a), we can see that the surface modes in (100) slab have different oscillation behavior; there is no clear periodic oscillation. However, from Fig. 5(b), we can clearly see that the surface modes in (111) slab have the similar oscillation behavior with the period of about three layers, i.e., the oscillatory period is the same as that of the interlayer relaxation, the surface energy, and the total DOS at the Fermi level in (111) slab, as discussed above. Recently, Yndurain and Jigato[15] found that the variation in surface phonon states with the slab thickness has the same bilayer period as that for the interlayer relaxation and the surface energy in Pb(111) thin films. Furthermore, we find that the oscillation of the surface modes in (111) slab has strong correlation with the oscillation of the interlayer relaxation. The frequencies of surface modes S_1 at $\bar{M}$ and $\bar{K}$ show maximum for $N=3,6,9$, while the topmost interlayer distances show minimum at the same slab thickness. The short interlayer distance leads to a stronger force constant and then increases the frequency.

Figure 6 shows the layer localized phonon DOS with respect to 12-layer (111) and (100) slabs together with the bulk phonon DOS. The phonon DOS of the middle layer of the two slabs is quite bulklike. For both two slabs, the surface-layer phonon DOS is significantly different from that of the middle layer. The vibrational frequencies of the surface-layer phonons shift downward relative to that of the middle layer, clearly implying that the surface-layer phonons soften. This softening is more visible in (100) slab. From Fig. 4(a), we know that there are two surface modes below the bulk con-

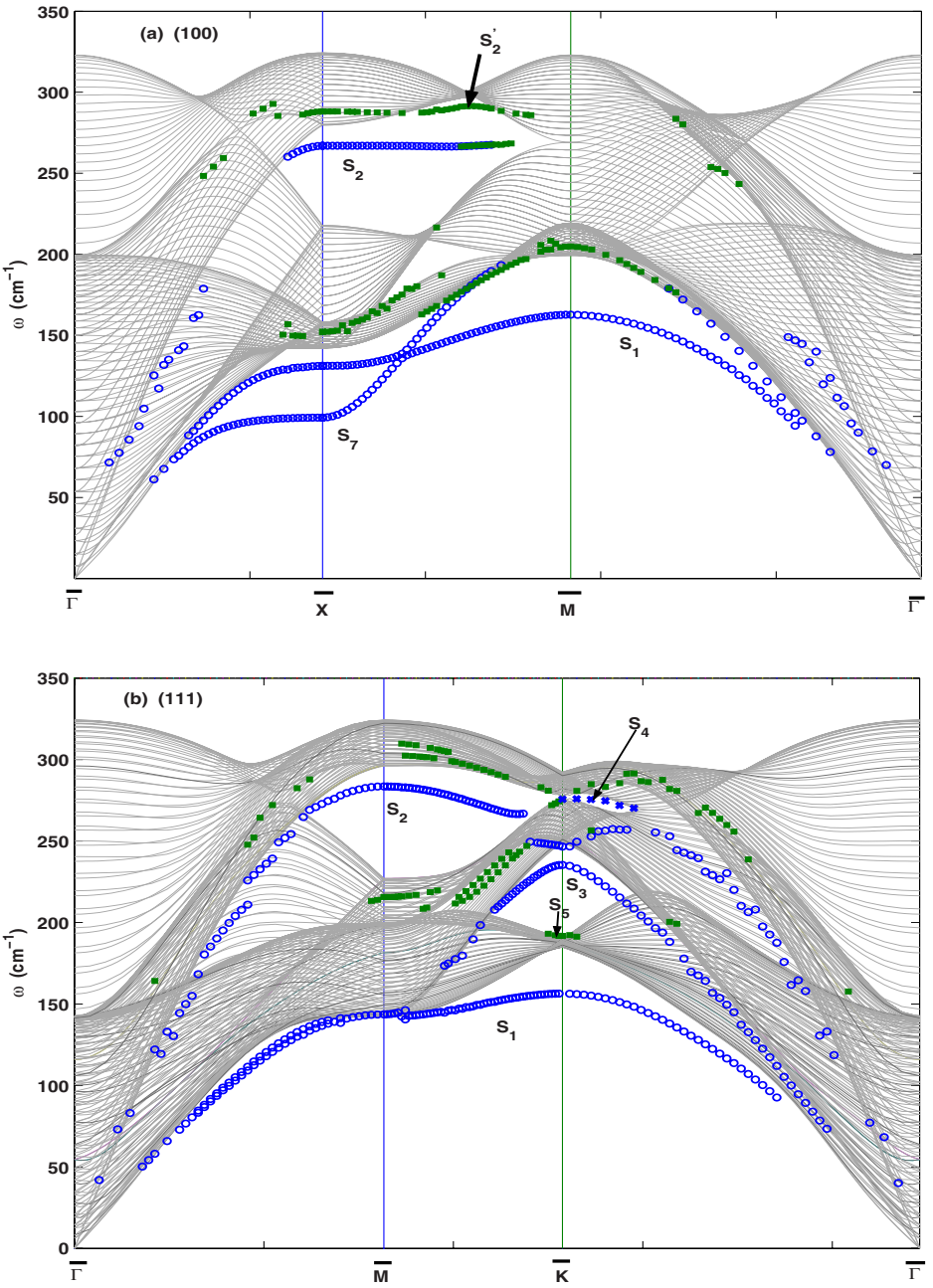

FIG. 4. (Color online) The localized surface phonon modes for the fully relaxed (a) 13-layer (100) slab and (b) 12-layer (111) slab. The light gray lines represent the projected bulk phonon dispersions. The surface modes localized in the first and second layers are indicated with open circles and filled squares, respectively.

tinuum bands. So, two peaks appear at the low-frequency side in the surface-layer phonon DOS curve of (100) slab.

After obtaining the phonon DOS, the root-mean-square (rms) displacement of atom can be calculated by the expression

$$\sqrt{\langle u_a^2 \rangle} = \left(\frac{\hbar}{M_a} \int \frac{F_a(\omega)\left[n(\omega) + \frac{1}{2} \right]}{\omega} d\omega \right)^{1/2}, \qquad (2)$$

where M_a is the mass of atom a, $F_a(\omega)$ is atom projected phonon DOS, and $n(\omega)=1/(e^{\hbar\omega/KT}-1)$ and is the phonon occupation number at a given temperature. Taking $T=300$ K, the obtained rms displacement is 0.252 a.u. for the bulk Al. For 12-layer (111) and (100) slabs, the obtained rms displacements for the atoms at the surface layer are 0.319 and 0.333 a.u., respectively. The rms value is nearly the same as that in the bulk for the atoms in the middle layers. From Eq. (2), we can see that the softening of surface-layer phonon results in larger rms displacement.

We shall now discuss the EP interaction. According to the Migdal-Eliashberg theory,[31] the phonon linewidth arises from the EP interaction by averaging over the Fermi surface and is given by

$$\gamma_{\mathbf{q}\nu} = 2\pi\omega_{\mathbf{q}\nu} \sum_{\mathbf{k}jj'} |g^{\mathbf{q}\nu}_{\mathbf{k}+\mathbf{q}j'\mathbf{k}j}|^2 \delta(\epsilon_{\mathbf{k}j} - \epsilon_F)\delta(\epsilon_{\mathbf{k}+\mathbf{q}j'} - \epsilon_F), \qquad (3)$$

where the EP matrix element $g^{\mathbf{q}\nu}_{\mathbf{k}+\mathbf{q}j'\mathbf{k}j}$ is determined self-consistently by the linear-response theory.[16,17] The $\mathbf{q}$-dependent EP coupling constant $\lambda_{\mathbf{q}\nu}$ for each mode can be obtained by dividing $\gamma_{\mathbf{q}\nu}$ by $\pi N(E_F)\omega^2_{\mathbf{q}\nu}$. The total EP cou-

TABLE I. Surface-mode frequencies (in meV) of Al(100) and Al(111) at selected high-symmetry points.

	$\bar{X}$			$\bar{M}$		
Al(100)	S_1	S_7	S_2	S_1		
	16.2	12.3	33.1	20.2		This work
	16.2	12.0	32.7	19.8		Ref. 25[a]
	14.9	12.4	33.5	20.3		Ref. 27
	16.1					Ref. 28
	$\bar{K}$			$\bar{M}$		
Al(111)	S_1	S_5	S_3	S_1	S_2	
	19.4	23.8	29.2	17.3	35.1	This work
	18.6			17.0	35.2	Ref. 29
	≈17.7			≈17.1		Ref. 30

[a]Determined from Fig. 1 in Ref. 25.

pling constant λ can be directly obtained by evaluating

$$\lambda = \sum_{\mathbf{q}\nu} \lambda_{\mathbf{q}\nu}. \tag{4}$$

After obtaining the EP coupling constant λ, the superconducting transition temperature T_C can be estimated using the McMillian expression,

$$T_C = \frac{\omega_{\ln}}{1.2} \exp\left\{ -\frac{1.04(1+\lambda)}{\lambda - \mu^*(1+0.62\lambda)} \right\}, \tag{5}$$

where μ^* is the Coulomb pseudopotential and $\omega_{\ln}$ is the logarithmically averaged frequency and defined by

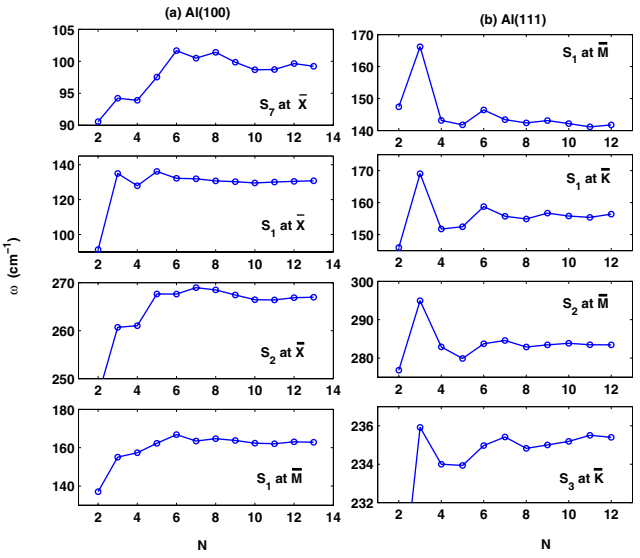

FIG. 5. (Color online) Frequencies of localized surface phonon modes as a function of the number of layers N in the slab (a) for Al(100) and (b) for Al(111).

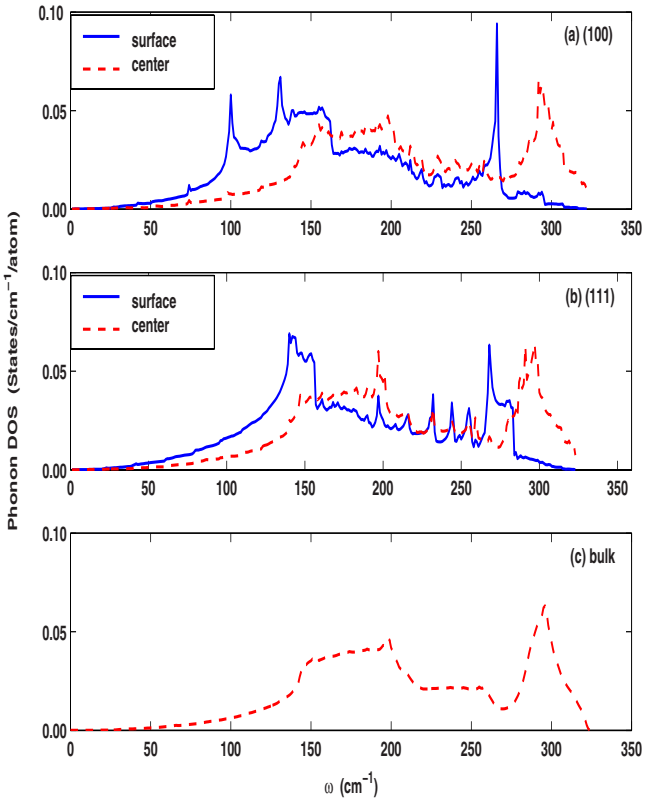

FIG. 6. (Color online) The layer localized phonon DOS with respective to (a) Al(100) and (b) Al(111), together with (c) Al bulk phonon DOS.

$$\omega_{\ln} = \exp\left\{ \frac{1}{\lambda} \sum_{\mathbf{q}\nu} \frac{\gamma_{\mathbf{q}\nu} \ln \omega_{\mathbf{q}\nu}}{\pi N(E_F)\omega_{\mathbf{q}\nu}^2} \right\}. \tag{6}$$

Taking a typical value for $\mu^*=0.12$, the calculated T_C together with the EP coupling constant as a function of film thickness are shown in Fig. 7. For both two slabs, we can see that the variation trend in the EP coupling-constant curve is nearly the same as that of T_C curve and there is an overall trend of decreasing T_C toward to the bulk value. For (100) slab, the oscillation behavior of λ and T_C is different from that of DOS curve and there is also no clear periodic oscillation. However, for (111) slab, we find that the oscillations of λ and T_C are nearly in phase with that of the total DOS at the Fermi level $N(E_F)$ with the period of about three layers. T_C has its minimum at $N=3,6,9,12$. Of course, the electron density of states is not the only factor affecting T_C. We notice that the oscillation of the surface phonon mode is exactly out of phase with that of $N(E_F)$ curve in (111) slab. In other words, when $N(E_F)$ has its maximum for some slab thicknesses, surface phonon modes soften obviously, which increases the EP coupling and enhances superconductivity further.

It is interesting to note that the values of λ and T_C obtained in this work at small N greatly exceed their bulk values. For example, the calculated (λ, T_C) are (1.01, 9.42) and (0.75, 6.81) for (100) and (111) slabs, respectively, at $N=2$, while their bulk values are (0.42, 1.04) which are close to the results (0.44, 1.39) of other calculation based on the full-

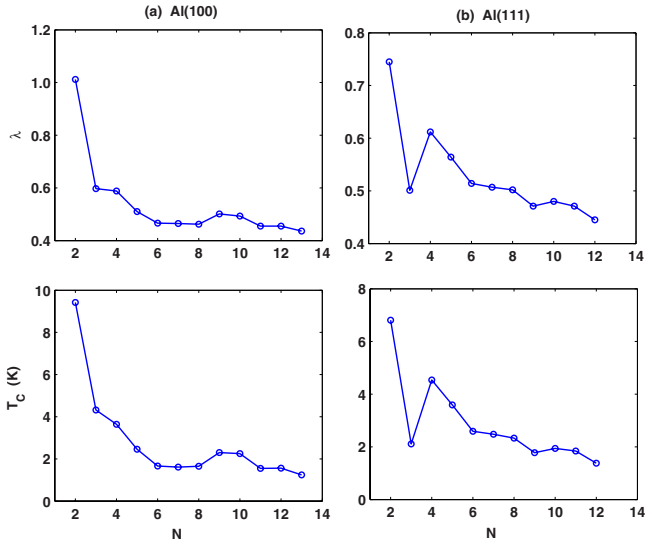

FIG. 7. (Color online) The calculated EP coupling constant λ and T_C as a function of the number of layers N in the slab (a) for Al(100) and (b) for Al(111).

potential linear muffin-tin orbital (LMTO) method.[32] Valla *et al.*[12] reported the peak of the EP coupling in ultrathin silver films deposited on a V(100) surface appears at $N=2$. The early investigation had shown that the regions of the highest T_C are within a few monolayers in both Al and Sn.[9] In Ref. 33, Bose *et al.* raised the two mechanisms used to account for the size dependence of T_C involving the softening of the phonon spectrum and the change in the electronic DOS due to discretization of the energy bands. This work confirms their suggestion by first-principles calculations. Both electronic and phonon confinements contribute to the enhancement of superconductivity for film at small thickness.

IV. SUMMARY

In summary, this work has reported a detailed investigation of the evolution of electronic structures, surface phonons, and EP interactions with the slab thickness in Al(100) and Al(111) superconductivity films. The calculated interlayer relaxations, surface energies, total DOS at the Fermi level, and even the surface phonon states oscillate with the period of about three layers for Al(111) films. However, the same behavior is not clearly found for Al(100) films. These differences between Al(111) and Al(100) films are discussed by considering the crystal band structure. Furthermore, the calculated λ and T_C have also an oscillatory variation with nearly three layers periodicity in Al(111) films. For both two slabs, the values of λ and T_C obtained in this work at small slab thickness greatly exceed their bulk values. Both electronic confinement and the softening of surface phonons contribute to the enhancement of superconductivity for films at small thickness.

ACKNOWLEDGMENTS

The author thanks Y. Xiong for a critical reading of the paper. This work was supported by the National Natural Science Foundation of China under Grant No. 10174011.

[1] A. E. Meyerovich and I. V. Ponomarev, Phys. Rev. B **67**, 165411 (2003).
[2] J. L. F. Da Silva, Phys. Rev. B **71**, 195416 (2005).
[3] G. Q. Huang, M. Liu, L. F. Chen, and D. Y. Xing, Phys. Lett. A **314**, 109 (2003).
[4] M. Jalochowski, M. Hoffmann, and E. Bauer, Phys. Rev. Lett. **76**, 4227 (1996).
[5] Y. F. Zhang, Z. Tang, T. Z. Han, X. C. Ma, J. F. Jia, Q. K. Xue, K. Xun, and S. C. Wu, Appl. Phys. Lett. **90**, 093120 (2007).
[6] J. J. Paggel, C. M. Wei, M. Y. Chou, D.-A. Luh, T. Miller, and T.-C. Chiang, Phys. Rev. B **66**, 233403 (2002).
[7] N. Binggeli and M. Altarelli, Phys. Rev. Lett. **96**, 036805 (2006).
[8] D.-A. Luh, T. Miller, J. J. Paggel, M. Y. Chou, and T.-C. Chiang, Science **292**, 1131 (2001).
[9] M. Strongin, O. F. Kammerer, J. E. Crow, R. D. Parks, D. H. Douglass, and M. A. Jensen, Phys. Rev. Lett. **21**, 1320 (1968).
[10] Y. Guo, Y. F. Zhang, X. Y. Bao, T. Z. Han, Z. Tang, L. X. Zhang, W. G. Zhu, E. G. Wang, Q. Niu, Z. Q. Qiu, J. F. Jia, Z. X. Zhao, and Q. K. Xue, Science **306**, 1915 (2004); Y. F. Zhang, J. F. Jia, T. Z. Han, Z. Tang, Q. T. Shen, Y. Guo, Z. Q. Qiu, and Q. K. Xue, Phys. Rev. Lett. **95**, 096802 (2005).
[11] D. Eom, S. Qin, M. Y. Chou, and C. K. Shih, Phys. Rev. Lett. **96**, 027005 (2006).
[12] T. Valla, M. Kralj, A. Šiber, M. Milun, P. Pervan, P. D. Johnson, and D. P. Woodruff, J. Phys.: Condens. Matter **12**, L477 (2000).
[13] D.-A. Luh, T. Miller, J. J. Paggel, and T.-C. Chiang, Phys. Rev. Lett. **88**, 256802 (2002).
[14] A. Eiguren, S. de Gironcoli, E. V. Chulkov, P. M. Echenique, and E. Tosatti, Phys. Rev. Lett. **91**, 166803 (2003).
[15] F. Yndurain and M. P. Jigato, Phys. Rev. Lett. **100**, 205501 (2008).
[16] S. Baroni, S. de Gironcoli, A. Dal Corso, and P. Giannozzi, Rev. Mod. Phys. **73**, 515 (2001).
[17] S. Baroni, S. de Gironcoli, A. Dal Corso, and P. Giannozzi (http://www.pwscf.org).
[18] D. Vanderbilt, Phys. Rev. B **41**, 7892 (1990).
[19] J. P. Perdew, K. Burke, and M. Ernzerhof, Phys. Rev. Lett. **77**, 3865 (1996).
[20] M. Methfessel and A. T. Paxton, Phys. Rev. B **40**, 3616 (1989).
[21] V. Fiorentini and M. Methfessel, J. Phys.: Condens. Matter **8**, 6525 (1996).
[22] C. M. Wei and M. Y. Chou, Phys. Rev. B **75**, 195417 (2007).
[23] T. Miller, A. Samsavar, G. E. Franklin, and T.-C. Chiang, Phys. Rev. Lett. **61**, 1404 (1988).
[24] C. M. Wei and M. Y. Chou, Phys. Rev. B **66**, 233408 (2002).
[25] V. Chis, B. Hellsing, G. Benedek, M. Bernasconi, and J. P. Toennies, J. Phys.: Condens. Matter **19**, 305011 (2007).
[26] R. E. Allen, G. P. Alldredge, and F. W. de Wette, Phys. Rev. B **4**, 1661 (1971).

[27] K.-P. Bohnen and K. M. Ho, Surf. Sci. **207**, 105 (1988).
[28] M. Gester, D. Kleinhesselink, P. Ruggerone, and J. P. Toennies, Phys. Rev. B **49**, 5777 (1994).
[29] J. Schöchlin, K.-P. Bohnen, and K. M. Ho, Surf. Sci. **324**, 113 (1995).
[30] A. Lock, J. P. Toennies, C. Wöll, V. Bortolani, A. Franchini, and G. Santoro, Phys. Rev. B **37**, 7087 (1988).
[31] P. B. Allen and B. Mitrovic, *Solid State Physics* (Academic, New York, 1982), Vol. 37, p. 1.
[32] S. Y. Savrasov and D. Y. Savrasov, Phys. Rev. B **54**, 16487 (1996).
[33] S. Bose, P. Raychaudhuri, R. Banerjee, P. Vasa, and P. Ayyub, Phys. Rev. Lett. **95**, 147003 (2005).